Pergamon

Int. J. Solids Structures Vol. 35, No. 21, pp. 2775–2793, 1998

0020-7683/98 $19.00 + .00

PII: S0020-7683(97)00195-9

FUNDAMENTAL CLOSED-FORM SOLUTIONS FOR SOLID AND THIN-WALLED COMPOSITE BEAMS INCLUDING A COMPLETE OUT-OF-PLANE WARPING MODEL

OMRI RAND
Faculty of Aerospace Engineering, Technion—Israel Institute of Technology, Haifa 32000, Israel

(*Received* 4 *February* 1997; *in revised form* 22 *June* 1997)

Abstract—A model for predicting the structural behavior of composite beams is presented. The model includes a three-dimensional warping distribution and is designed to handle arbitrary solid cross-sections or general thin-walled geometries. The formulation enables the derivation of fundamental strength-of-materials type closed-form analytic solutions for various basic composite beam configurations and loading modes. These fundamental solutions explicitly identify the origin of the elastic couplings and supply educating insight into the structural mechanisms in composite beams. In addition, the detailed distributions of the out-of-plane warping provided by the present analytic solutions for relatively simple geometries may be used as the basic shear deformation shape functions in numerical analyses of more complex configurations. © 1998 Elsevier Science Ltd. All rights reserved.

1. INTRODUCTION

Composite beams are major components in many engineering applications. Among the various advantages offered by composites, it is important to mention their high strength to weight ratio, their preferred fatigue characteristics and the relatively simple techniques that are required for their producing and shaping.

The elastic couplings in orthotropic laminae emerge from the material level that exhibits couplings between normal stress and shear strain and between shear stress and normal strain. However, the present analysis is aimed towards the fundamental modeling, solution and understanding of the coupling mechanisms in composite beams in the structural level. In this level, composite beams that consist of orthotropic laminae that are not aligned with their longitudinal axis, exhibit couplings between the components of the transverse curvature, the twist and the axial (extension) strain. Elastic couplings may be exploited for "passive" improvement of both the static and the dynamic characteristics of composite beams. Improvement of the vibratory characteristics and augmentation of the stability margins of helicopter blades are examples for potential applications that may benefit from elastic couplings (see for example Yuan *et al.*, 1994).

The analysis of composite beams has been originated from the classical lamination theory by modification of the material constitutive relations (see for example Ambartsmyan, 1964; Tsai and Hahn, 1980; Ochoa and Reddy, 1992). Consequently, the resulting models were originally suitable for thin plates and in many cases, the term "composite beam" still refers to a slender thin beam ("plate-beam" models). It may be shown that adequate prediction of the elastic couplings must be based on a detailed modeling of the distortion of planes perpendicular to the beam axis before deformation. This shear deformation distribution will be also referred to as "out-of-plane warping" in what follows. Hence, due to the important role played by the warping in the overall behavior of the beams and in particular in the determination of the coupling mechanisms, the above models were improved by "higher-order shear deformation theories" (see for example Noor and Burton, 1989; Nosier and Reddy, 1992). Yet, most of these models are limited since they are valid for relatively thin plates of rectangular cross-sections and may handle bending in one

direction only. Discussion and numerical study of the importance of various shear deformation models may be found in Chandrashekhara and Bangera (1992) and Maiti and Sinha (1994).

Since the warping is a local characteristic, detailed numerical models are typically based on enormous number of degrees of freedom. Simon (1981), Giavotto *et al.* (1983) and Stemple and Lee (1989) described representative numerical schemes that are based on relatively large number of degrees of freedom and include the necessary warping features. However, such models impose limitations on their usage in comprehensive analyses, such as multi-disciplinary optimizations, where many evaluations of the structural analysis are required. Moreover, detailed numerical models that are capable of providing the required prediction of the warping do not always supply enough insight into the structural mechanisms, which limits designers intuition in new problems and in improving existing configurations. Additional common way of analyzing composite beam behavior is based on a two-dimensional analysis of a representative cross-section, e.g. Kosmatka and Friedmann (1989). The outcome of such analysis are the cross-sectional stiffness and coupling terms which are fed into a one-dimensional beam analysis. Further common simplifications of numerical models are based on assumed warping shape functions, and most of them take into account only the torsional-related warping effects and constant transverse shear distributions. Discussion of such models may be found in Librescu and Song (1991) and Schmidt and Librescu (1994). Additional discussion and various composite beam models may be found in Bull (1995).

Berdichevsky *et al.* (1992) present some analytic approach for thin-walled beams which is based on variationally and asymptotically theory. However, unlike the well-known "strength of materials" solution for isotropic beams, there are no fundamental closed-form exact analytic solutions for composite beams. Such solutions have the potential to provide an analytic insight and a clear identification of the major parameters that control the composite beam behavior and the resulting structural couplings.

The model presented in this paper is confined to the linear case. Most of the closed-form solutions apply to homogeneous solid cross-sections of arbitrary geometry. As will be shown further on, these solutions may be generalized for much more extensive use. In addition, by supplying the exact shear deformation distributions for different basic cases, the analytic solutions of the present paper provide guidelines for numerical schemes that are based on various types of built-in shear deformation shape functions. All the examples presented in this paper are for the typical material properties presented in Appendix A.

2. GOVERNING EQUATIONS FOR SOLID AND THIN-WALLED COMPOSITE BEAMS

A straight and untwisted composite beam is shown in Fig. 1(a). The beam length, l, is measured along the x coordinate line while the coordinates y and z define the cross-sectional planes. Schemes of solid and thin-walled cross-sections are presented in Fig. 1(b) and (c), respectively. In the case of a solid cross-section, it is assumed that the orthotropic laminae are parallel to the x–y plane. For a thin-walled cross-section, the orientation of the orthotropic laminae is assumed to coincide with the local wall direction.

The deformation assumption is based on two types of displacements. First, since a "beam-like behavior" is expected, cross-sectional displacements $u(x)$, $v(x)$ and $w(x)$ in the x-, y- and z-directions, respectively, and a twist angle, $\phi(x)$, about the x-direction are defined. These components of the deformation are functions of x only, and therefore they represent "rigid" displacements of each cross-section that contains no warping. To account for the out-of-plane warping, a three-dimensional warping function is superimposed (in the x-direction) upon the above mentioned displacements. This warping function is denoted Ψ, and is assumed to be of zero average value over the cross-sectional area (i.e. $\int\int \Psi \, dA = 0$). For solid cross-sections, Ψ is a function of x, y and z, and for thin-walled cross-sections, Ψ is a function of x and s, where s is a circumferential coordinate along the wall [see Fig. 1(c)]. Hence, the variation of Ψ through the wall thickness is neglected. This assumption is compatible with the common plane-stress approximation for thin plates.

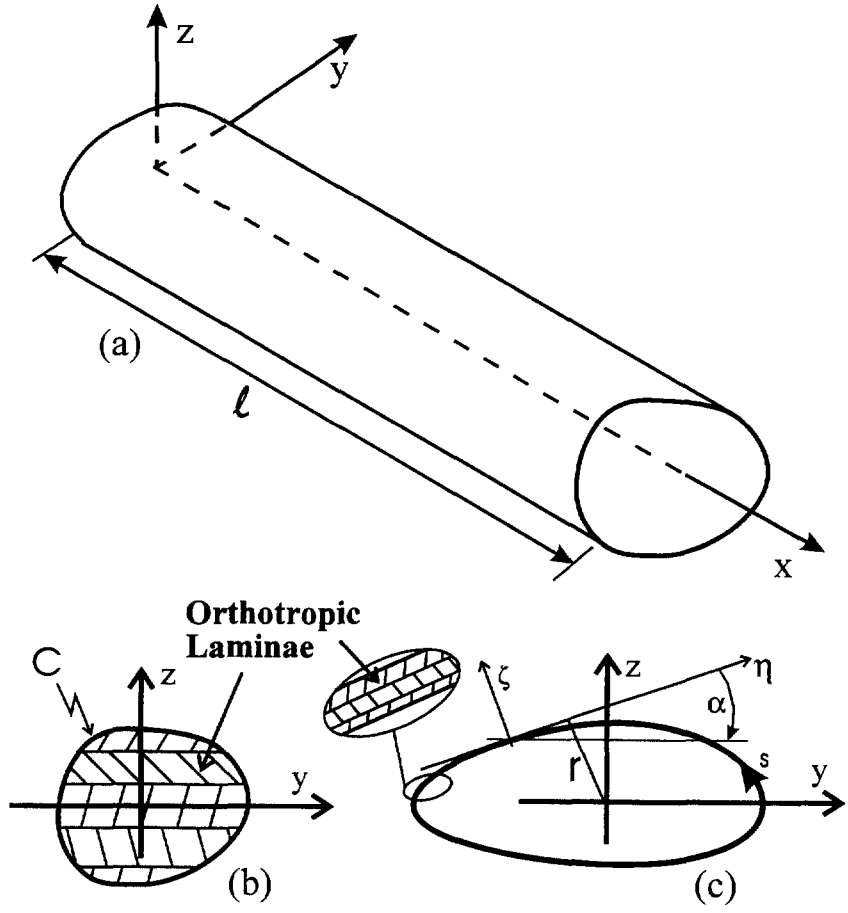

Fig. 1. Composite beam notation. (a) A straight beam before deformation. (b) An orthotropic solid cross-section. (c) An orthotropic thin-walled cross-section.

Since the linear formulation requires no distinction between the deformed and undeformed direction, the above assumed deformation components may be directly used to construct the strain expressions. Considering this linear case, the nonvanishing strain components for a solid cross-section are given by

$$\varepsilon_{xx} = u_{,x} - yv_{,xx} - zw_{,xx} + \Psi_{,x} \tag{1a}$$

$$\gamma_{xz} = y\phi_{,x} + \Psi_{,z} \tag{1b}$$

$$\gamma_{xy} = -z\phi_{,x} + \Psi_{,y} \tag{1c}$$

where ε_{xx} is the normal strain, and γ_{xz}, γ_{xy} are the shear strains. $()_{,x}$ denotes differentiation with respect fo x. For a thin-walled cross-section, it is convenient to define a local system of coordinates which is attached to the contour so that ξ is parallel to the x-direction and η is tangent to the local contour—see Fig. 1(c). The angle α is measured between the y- and the η-directions, and r is the normal distance to the tangent to the contour at the point under discussion. Thus, in this case, the only nonzero strain components are the normal strain, $\varepsilon_{\xi\xi}$, and the shear strain along the wall, $\gamma_{\xi\eta}$, which are given by

$$\varepsilon_{\xi\xi} = u_{,x} - yv_{,xx} - zw_{,xx} + \Psi_{,x} \tag{2a}$$

$$\gamma_{\xi\eta} = -r\phi_{,x} - \Psi_{,s} \tag{2b}$$

The general constitutive relations for a general orthotropic lamina consists of nine independent elastic moduli (see for example Tsai and Hahn, 1980; or Ochoa and Reddy, 1992). Reduction of these relations for the present case of solid cross-sections is obtained by exploiting the beam slenderness and assuming $\sigma_{yy} = \sigma_{zz} = \tau_{yz} = 0$. This assumption has been proved to be exact in the isotropic case (see Sokolnikoff, 1956), and serves here as an approximation that has been proved to be adequate in many shear-deformation based models. Elimination of this assumption requires the inclusion of the in-plane warping as well which is beyond the scope of the present model. Consequently, it is possible to express the relations between the stress components that act over a solid cross-sectional area and the above strain components by

$$\begin{pmatrix} \sigma_{xx} \\ \tau_{xz} \\ \tau_{xy} \end{pmatrix} = \begin{bmatrix} C_{11} & 0 & C_{16} \\ 0 & C_{55} & 0 \\ C_{16} & 0 & C_{66} \end{bmatrix} \begin{pmatrix} \varepsilon_{xx} \\ \gamma_{xz} \\ \gamma_{xy} \end{pmatrix} \tag{3}$$

where the elastic moduli C_{ij} are functions of the material properties and the local ply angle relative to the x-axis. Note that the strains ε_{yy}, ε_{zz} and γ_{yz} are not zero (these strains may be determined based on the values of the stress components σ_{xx}, τ_{xz} and τ_{xy}), and thus, Poisson's ratio effect is included in the present formulation.

For a thin-walled cross-section, the above constitutive relations are applicable in the local ξ, η, ζ system directions. By assuming $\sigma_{\zeta\zeta} = \tau_{\xi\zeta} = \tau_{\eta\zeta} = 0$ which is compatible with the plane-stress assumption, in addition to $\sigma_{\eta\eta} = 0$ which is justified due to the neglect of the in-plane warping (i.e. the cross-sectional shape remains "rigid"), these relations may be reduced to

$$\begin{pmatrix} \sigma_{xx} \\ \tau_{\xi\eta} \end{pmatrix} = \begin{bmatrix} C_{11} & C_{16} \\ C_{16} & C_{66} \end{bmatrix} \begin{pmatrix} \varepsilon_{\xi\xi} \\ \gamma_{\xi\eta} \end{pmatrix} \tag{4}$$

Equilibrium is achieved by four integral equations and one differential equation. The integral equations equate the cross-sectional resultants P (in the x-direction), F_y (in the y-direction), F_z (in the z-direction) and the moment resultant M_x (in the x-direction) that are induced by the external resultant loads to the corresponding loads obtained by the stress integrations. For solid cross-sections these four equations take the form

$$(P, F_y, F_z, M_x) = \int\int_A (\sigma_{xx}, \tau_{xy}, \tau_{xz}, \tau_{xz}y - \tau_{xy}z)\, \mathrm{d}A \tag{5}$$

where A is the cross-sectional area. The differential equation of equilibrium for solid cross-sections is the associated differential equilibrium equation in x-direction which is given by

$$\sigma_{xx,x} + \tau_{xy,y} + \tau_{xz,z} + B_x = 0 \tag{6}$$

where B_x is the body force in x-direction. To assure consistency of the above integral and differential equations in the x-direction, one should require $P_{,x} = -\int\int B_x\, \mathrm{d}A$. Similarly, the corresponding cross-sectional equilibrium equations may be written for a thin-walled cross-section as

$$(P, F_y, F_z, M_x) = \int_s \int_t (\sigma_{\xi\xi}, \tau_{\xi\eta}\cos\alpha, \tau_{\xi\eta}\sin\alpha, -r\tau_{\xi\eta})\, \mathrm{d}\zeta\, \mathrm{d}s \tag{7}$$

while the differential equilibrium equation [eqn (6)] becomes

$$\sigma_{\xi\xi,\xi} + \tau_{\xi\eta,\eta} + B_\xi = 0 \tag{8}$$

There are eight beam-type boundary conditions at the beam root and tip. For a clamped–free beam, six of them are following geometrical boundary conditions at the beam root:

$$u = v = v_{,x} = w = w_{,x} = \phi = 0 \tag{9}$$

The remaining two natural boundary conditions at the beam tip are based on equating the external transverse tip moments, M_y^t, M_z^t, to those obtained by stress integrations over the tip cross-sectional area A^t. These conditions may be written as

$$(M_y^t, M_z^t) = \int\int_{A^t} (\sigma_{xx} z, -\sigma_{xx} y)\, \mathrm{d}A^t \tag{10}$$

where in the case of thin-walled cross-section, σ_{xx} should be replaced by $\sigma_{\xi\xi}$. For solid cross-sections there is an additional contour boundary condition that ensures traction-free surface along the beam, namely

$$\tau_N = 0 \quad \text{on} \quad C \tag{11}$$

where τ_N is the shear stress normal to the contour C [see Fig. 1(b)]. No such boundary condition is required for thin-walled cross-section since $\tau_{\xi\zeta}$ is neglected.

As shown, the above formulation consistently includes body forces in the x-direction, and therefore may adequately be used to predict also the effect of rotation on the behavior of composite beams.

3. ANALYTIC SOLUTIONS FOR BEAMS OF SOLID CROSS-SECTIONS

The analytic solutions presented in this section are for homogeneous solid cross-sections. In this context, a homogeneous cross-section is the case where all laminae are identical and oriented at the same angle with respect to the x-axis, or the case of a single lamina cross-section. From an analytic point of view, this case is useful since the elastic moduli are all constants.

The following solutions were generated using well-established analytic technique that is based on a preliminary "assumption" of the solution form using unknown parameters. Further on, these parameters are determined so that the governing equations are fulfilled in an exact manner. Thus, once such a procedure is successfully completed, the resulting solution is unique, exact and contains no arbitrary assumptions.

3.1. *Axial load*

The solution of a cross-section of solid arbitrary geometry undergoing axial load is considered in this section. In order to be compatible with the above formulation, the load is assumed to emerge from a tip tensile force, P^t, and a body force distribution $B_x(x)$ which is assumed to be constant over the cross-sectional area. Therefore, the axial resultant force, $P(x)$, is obtained by integrating the equation $P_{,x} = -B_x A$ under the condition $P_{(x=l)} = P^t$, where l is the beam length.

The solution for this case may be generated by assuming $w = \phi = 0$ and a warping function of the form $\Psi = \alpha(x)y$, where $\alpha(x)$ is a longitudinal function to be determined. Substituting the above assumption into eqns (1a–c) yields

$$\varepsilon_{xx} = u_{,x} - y v_{,xx} - \alpha_{,x} y \tag{12a}$$

$$\gamma_{xz} = 0 \tag{12b}$$

$$\gamma_{xy} = \alpha \tag{12c}$$

Using eqn (3) the stresses in this case become

$$\sigma_{xx} = C_{11}(u_{,x} - yv_{,xx} - \alpha_{,x}y) + C_{16}\alpha \tag{13a}$$

$$\tau_{xy} = C_{16}(u_{,x} - yv_{,xx} - \alpha_{,x}y) + C_{66}\alpha \tag{13b}$$

Integrating eqn (13a, b) for a system of coordinate that is located at the center of the cross-sectional area (i.e. $\int\int y\,dA = \int\int z\,dA = 0$), using $F_y = 0$ [see eqn (5)], shows that $u_{,x}$ and α are given by

$$u_{,x} = P(x)\frac{C_{66}}{A(C_{11}C_{66} - C_{16}^2)} \tag{14a}$$

$$\alpha = P(x)\frac{C_{16}}{A(C_{11}C_{66} - C_{16}^2)} \tag{14b}$$

In addition, to satisfy the differential equilibrium equation [eqn (6)], the chordwise curvature is assumed to be given by $v_{,xx} = -\alpha_{,x}$. With this assumption, eqns (13) and (14) show that $\sigma_{xx} = P/A$ and $\tau_{xy} = 0$, which, with the aid of the above-mentioned distribution of the body force (i.e. $B_x = -P_{,x}/A$), satisfy the differential equilibrium equation. Then, $u(x)$ is obtained by integrating eqns (14a, b) with the boundary conditions of eqn (9).

The above solution yields some interesting observations. First, considering the simple case of a tip axial load (i.e. $B_x = 0$ and $P(x) = P^t$), eqn (14a) indicates that the longitudinal strain variation is influenced by C_{11}, C_{66} and C_{16}. Thus, the approximation $u_{,x} \cong P^t/AC_{11}$ which is commonly used in such cases may induce significant discrepancies. For the material properties of Appendix A, an error of about 50% is obtained by this approximation for a ply angle of 30°. It is therefore clear that the reduction in the axial stiffness for nonzero lamination angle is not represented solely by the reduction in the value of C_{11}.

The present solution also indicates that the assumed linear shear deformation over the cross-section is indeed valid. The warping in this case varies longitudinally as $P(x)$ and is therefore proportional to $yP(x)$. In addition, eqns (12a, c), (14a, b) show that the shear strain may be written as $\gamma_{xy} = (C_{16}/C_{66})\varepsilon_{xx}$, which indicates that it might reach values in the order of the axial strain $\varepsilon_{xx}(=u_{,x})$.

It should also be mentioned that the chordwise curvature $v_{,xx}$ emerge solely from the warping longitudinal derivative $\alpha_{,x}$ (in other words, the above solution remains valid, if both $v_{,xx}$ and $\alpha_{,x}$ are neglected). Warping longitudinal derivatives are therefore essential for capturing the edgewise curvature induced in this case.

3.2. *Tip moments*

The case of a beam undergoing tip moments M_x^t, M_y^t and M_z^t (in the x-, y- and z-directions, respectively), is unique in the sense that the curvature components $(w_{,xx}, v_{,xx})$, the twist $(\phi_{,x})$ and the axial strain $(u_{,x})$ are constants along the beam (it is therefore also clear that $M_x = M_x^t$, $M_y = M_y^t$ and $M_z = M_z^t$ in this case). To derive an exact solution for this case for a solid homogeneous cross-section of arbitrary geometry, the uncoupled case is first examined. The uncoupled case is obtained by setting C_{16} to zero, and keeping the remaining elastic moduli C_{11}, C_{66} and C_{55} unchanged. In this case, bending and torsion are not coupled and the torsional moment, M_x^t, is the only contributor to the warping. Here, it is convenient to adopt the closed-form analytic solution procedure of Sokolnikoff (1956), that yields the torsional rigidity, D (defined by $M_x^t/\phi_{,x}$) and the associated two-dimensional warping function $\varphi(y, z)$.

Having D and $\varphi(y, z)$ for the uncoupled case, the twist and the warping in the coupled case are assumed to be of the following form:

$$\phi_{,x} = \frac{M_x^t}{D} - \frac{C_{16}}{2C_{66}} w_{,xx} \tag{15a}$$

$$\Psi = \frac{M_x^t}{D}\varphi(y,z) + \frac{C_{16}}{2C_{66}}\left[w_{,xx}yz + v_{,xx}\left(y^2 - \frac{a^2}{12}\right) - 2u_{,x}y\right] \tag{15b}$$

which also ensures zero average warping distribution when the origin of the system of coordinates is placed at the center of the cross-sectional area. Based on eqns (1a–c), the strains in this case become

$$\varepsilon_{xx} = u_{,x} - yv_{,xx} - zw_{,xx} \tag{16a}$$

$$\gamma_{xz} = \frac{M_x^t}{D}(\varphi_{,z} + y) \tag{16b}$$

$$\gamma_{xy} = \frac{M_x^t}{D}(\varphi_{,y} - z) - \frac{C_{16}}{C_{66}}(u_{,x} - yv_{,xx} - zw_{,xx}) \tag{16c}$$

Therefore, according to eqn (3), the stresses are given by

$$\sigma_{xx} = \left(C_{11} - \frac{C_{16}^2}{C_{66}}\right)(u_{,x} - yv_{,xx} - zw_{,xx}) + C_{16}\frac{M_x^t}{D}(\varphi_{,y} - z) \tag{17a}$$

$$\tau_{xz} = C_{55}\frac{M_x^t}{D}(\varphi_{,z} + y) \tag{17b}$$

$$\tau_{xy} = C_{66}\frac{M_x^t}{D}(\varphi_{,y} - z) \tag{17c}$$

By definition, the shear stresses in this case are identical to the stresses obtained in the uncoupled case due to a tip torsional moment. Thus, the contour boundary condition [eqn (11)] is satisfied, and it is also clear that the force resultants F_y and F_z are zero [see eqn (5)]. Since $\sigma_{xx,x} = 0$ in this case, the differential equilibrium equation [eqn (6)] is satisfied exactly as in the uncoupled case. Adequate integrations of the normal stress σ_{xx} should be carried out to satisfy the integral equation for the axial resultant load [$P = 0$ in eqn (5)], and to satisfy the natural boundary conditions [eqn (10)] at the tip (note that in the present case, the above integrations are identical for all cross-sections). This step yields the following values of $u_{,x}$, $v_{,xx}$ and $w_{,xx}$:

$$\begin{pmatrix} u_{,x} \\ v_{,xx} \\ w_{,xx} \end{pmatrix} = \begin{bmatrix} A & -I_y & -I_z \\ I_y & -I_{yy} & -I_{yz} \\ I_z & -I_{yz} & -I_{zz} \end{bmatrix}^{-1} \begin{pmatrix} -C_{16}\dfrac{M_x^t}{D}(I_\varphi - I_z) \\ -M_z^t - C_{16}\dfrac{M_x^t}{D}(I_{\varphi y} - I_{yz}) \\ M_y^t - C_{16}\dfrac{M_x^t}{D}(I_{\varphi z} - I_{zz}) \end{pmatrix} \frac{C_{66}}{C_{11}C_{66} - C_{16}^2} \tag{18}$$

where

$$(A, I_y, I_z, I_{yz}, I_{yy}, I_{zz}, I_\varphi, I_{\varphi y}, I_{\varphi z}) = \iint_A \left(1, y, z, yz, y^2, z^2, \frac{\partial\varphi}{\partial y}, y\frac{\partial\varphi}{\partial y}, z\frac{\partial\varphi}{\partial y}\right) \mathrm{d}A \tag{19}$$

To simplify the above general expressions, the origin of the system of coordinates is assumed to be located at the cross-sectional area center, yielding $I_y = I_z = 0$. In addition, integrating

eqn (17c) over the cross-sectional area using $F_y = 0$, shows that $I_{\varphi} = 0$ in this case. In addition, for a cross-section that exhibits symmetry about the z-axis, it may be shown that $I_{yz} = I_{\varphi y} = 0$. For such cases, eqns (15a), (18) and (19) show that $u_{,x} = 0$ and

$$v_{,xx} = \frac{M_z^t}{I_{yy}} \frac{C_{66}}{C_{11}C_{66} - C_{16}^2} \tag{20a}$$

$$w_{,xx} = -\left[r_z \frac{C_{16} M_x^t}{D} + \frac{M_y^t}{I_{zz}} \right] \frac{C_{66}}{C_{11}C_{66} - C_{16}^2} \tag{20b}$$

$$\phi_{,x} = \frac{M_x^t}{D} \left[1 + \frac{C_{16}^2}{2(C_{11}C_{66} - C_{16}^2)} r_z \right] + \frac{M_y^t}{2I_{zz}} \frac{C_{16}}{C_{11}C_{66} - C_{16}^2} \tag{20c}$$

where r_z is a nondimensional parameter given by

$$r_z = 1 - \frac{I_{\varphi z}}{I_{zz}} \tag{21}$$

According to eqn (15b), the warping in this case may be written as

$$\Psi = \frac{M_x^t}{D} \varphi(y,z) - \frac{1}{2} \left[r_z \frac{C_{16} M_x^t}{D} + \frac{M_y^t}{I_{zz}} \right] \frac{C_{16}}{C_{11}C_{66} - C_{16}^2} yz + \frac{1}{2} \frac{M_z^t}{I_{yy}} \frac{C_{16}}{C_{11}C_{66} - C_{16}^2} \left(y^2 - \frac{a^2}{12} \right) \tag{22}$$

Integrating eqns (20a–c) using the geometric boundary conditions [eqn (9)], yields the displacement distribution over the beam. Clearly, for the case of a uniform clamped beam, $w(x) = (1/2)w_{,xx}x^2$, $v(x) = (1/2)v_{,xx}x^2$ and $\phi(x) = \phi_{,x}x$.

As indicated by eqns (20b, c), r_z controls the torsion–bending coupling and its value may be obtained by determining $\varphi(y,z)$ according to the solution procedure of Sokolnikoff (1956) and eqns (19) and (21). It turns out that r_z may be expressed as a function of a nondimensional parameter, q, that combines geometry and elastic characteristics and is given by

$$q = \frac{a}{b} \sqrt{\frac{C_{55}}{C_{66}}} \tag{23}$$

while it is possible to show that $r_z(1/q) = r_z(q)/q^2$. For a rectangular solid cross-section defined by the lines $y = \pm a/2$ and $z = \pm b/2$, it may be shown that $\partial\varphi/\partial y$ is given by:

$$\frac{2}{b} \frac{\partial \varphi^R}{\partial y} = \tilde{z} - \frac{16}{\pi^2} \sum_{n=1,3,5\ldots} \frac{1}{n^2} (-1)^{\frac{n-1}{2}} \left[1 - \frac{\cosh(n\pi q \tilde{y}/2)}{\cosh(n\pi q/2)} \sin(n\pi \tilde{z}/2) \right] \tag{24}$$

where $\tilde{y} = 2y/a$ and $\tilde{z} = 2z/b$. Using eqns (19), (21) and (23), r_z for this case takes the form

$$r_z^R = 2 - \frac{192}{q\pi^4} \sum_{n=0}^{\infty} \frac{(-1)^n}{(2n+1)^4} \tanh(mq) \left[\frac{1}{m} \sin(m) - \cos(m) \right] \tag{25}$$

where $m = \pi(2n+1)/2$.

For elliptic solid cross-section the contour of which is passing through $(y = \pm a/2, z = 0)$ and $(y = 0, z = \pm b/2)$, $\partial\varphi/\partial y$ is given by

$$\frac{2}{b}\frac{\partial \varphi^{E}}{\partial y} = \bar{z}\left[1 - \frac{2q^2}{1+q^2}\right] \tag{26}$$

and the following simple expression for r_z is obtained:

$$r_z^{E} = \frac{2q^2}{1+q^2} \tag{27}$$

Figure 2 presents the variation of r_z as a function of q for rectangular and elliptic cross-sections. As shown, r_z is a monotonic increasing function of q and is bounded by $0 \leqslant r_z \leqslant 2$. For a thin cross-section ("plate-beam" model), high values of q are obtained yielding $r_z \cong 2$. For a transversely isotropic type case where $C_{55} \cong C_{66}$, eqn (20b) shows that for the same elastic moduli and uncoupled torsional rigidity, the amount of bending due to torsional moment is reduced by more than 50% in a square cross-section (where $q \cong 1$ and $r_z \cong 0.84$) compared with a thin cross-section (where $q > 4$ and $r_z > 1.68$).

Typical warping and normal stress distributions induced by a tip torsional moment are presented in Fig 3(a, b). It is interesting to note that although the average normal stress vanishes (since this is a pure torsion case), it exhibits linear variation with respect to z along the $y = \pm a/2$ contour lines as observed in isotropic bending.

Examination of eqns (20 b, c) also shows that the ratio of the additional twist to the beamwise curvature induced by the composite couplings in the case of tip torsional moment is given by

$$\frac{\Delta\phi_{,x}}{w_{,xx}} = -\frac{C_{16}}{2C_{66}} \tag{28}$$

The same ratio is obtained in the case of beamwise tip moment (M_y^t) between the resulting twist and bending curvature (i.e. $\phi_{,x}/w_{,xx}$). It may be therefore concluded that in the case of a solid homogeneous beam, the bending–torsion coupling is controlled by the $-C_{16}/2C_{66}$

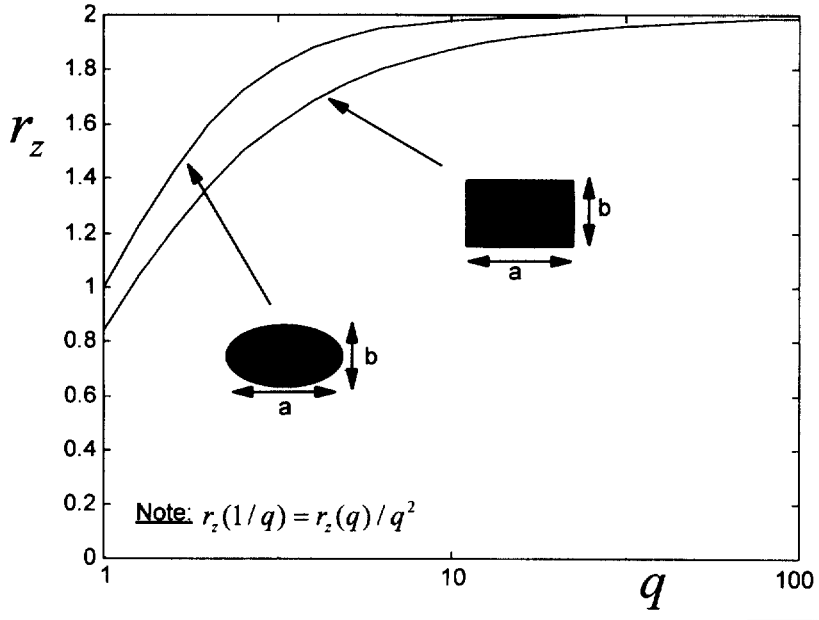

Fig. 2. The variation of r_z for solid rectangular and elliptic cross-sections ($q = a/b\sqrt{C_{55}/C_{66}}$).

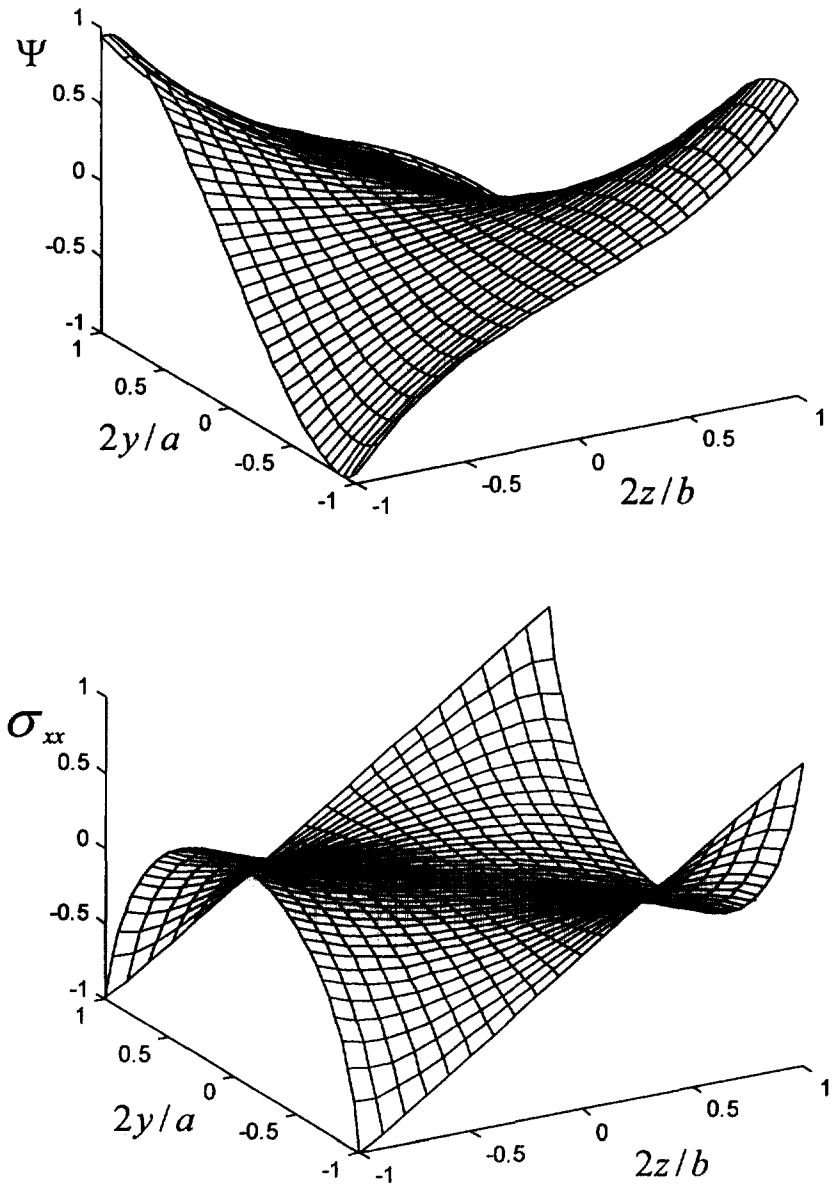

Fig. 3. (a) Warping distribution (normalized by the maximal absolute value) over the mid-span cross-section of a rectangular solid beam (defined by the lines $y = \pm a/2$ and $z = \pm b/2$) due to a tip torsional moment M_x'. For this case $a/l = 0.05$, $b/l = 0.025$ and the lamination angle is 10°. (b) Normal stress distribution (normalized by the maximal absolute value) over the mid-span cross-section of a rectangular solid beam (defined by the lines $y = \pm a/2$ and $z = \pm b/2$) due to a tip torsional moment M_x'. For this case $a/l = 0.05$, $b/l = 0.025$ and the lamination angle is 10°

ratio regardless any geometrical parameters. Additional support for this result and discussion are presented later on.

Figure 4 presents the variation of the uncoupled torsional rigidity, D, as a function of the lamination angle for a rectangular cross-section defined by the lines $y = \pm a/2$ and $z = \pm b/2$. As shown, without the bending–torsion coupling modulus (C_{16}), the torsional rigidity increases to a maximum value at the vicinity of 30° due to the augmented shear modulus C_{66} obtained at this lamination angle. However, when the bending–torsion coupling modulus C_{16} is not zero, eqn (20c) shows that the effective torsional rigidity, D_e, may be written as

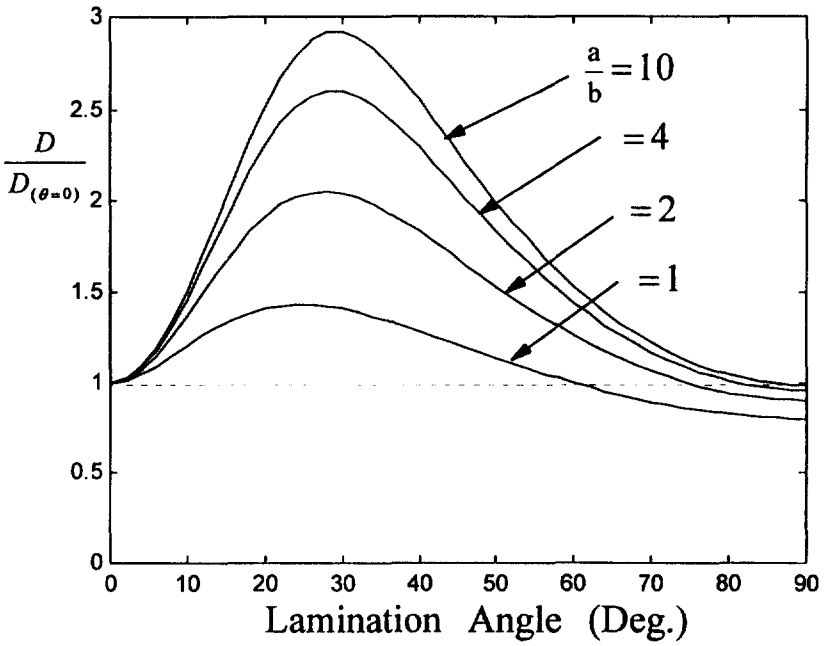

Fig. 4. The variation of the uncoupled torsional rigidity, D, as a function of the lamination angle for a rectangular cross-section defined by the lines $y = \pm a/2$ and $z = \pm b/2$.

$$\frac{D_e}{D} = \frac{1 - \dfrac{C_{16}^2}{C_{11}C_{66}}}{1 - \dfrac{C_{16}^2}{C_{11}C_{66}}\left(1 - \dfrac{r_z}{2}\right)} \tag{29}$$

Clearly, $D_e/D < 1$ and the loss of torsional rigidity is evident. The effective torsional rigidity may be reduced by 50% for lamination angle of about 25° and $a/b = 10$, since r_z is relatively large in this case. Note that this reduction is due to the elastic coupling and not due to geometric considerations (the torsional rigidity in the uncoupled case, D, is a function of a/b by itself—see Fig. 4). Overall, it may be concluded that the augmentation in the torsional rigidity obtained by the lamination angle is significantly decreased due to the presence of the coupling modulus C_{16}.

3.3. *Tip transverse forces*

The analytic solutions presented in this section are for a rectangular cross-section bounded by $y = \pm a/2$ and $z = \pm b/2$. In contrast with the previous cases of tip moments, tip transverse forces induce variations in the bending curvature along the beam, and a different type of solution is required.

3.3.1. *A tip beamwise force* (F_z^t). The solution in this case is initiated by assuming $u = v = 0$, and a warping function that is a sum of "isotropic" warping function and the warping obtained above due to M_y^t, namely

$$\Psi = -\frac{6F_z^t}{ab^3C_{55}}\left[\frac{z^3}{3} - \left(\frac{b}{2}\right)^2 z\right] - \phi_{,x}yz \tag{30}$$

If the $\Psi_{,x}$ term in eqn (2a) is neglected, eqns (1a–c) and (3) show that the resulting stresses are given by

$$\sigma_{xx} = -z(C_{11}w_{,xx}+2C_{16}\phi_{,x}) \tag{31a}$$

$$\tau_{xz} = -\frac{6F_z^t}{ab^3}\left[z^2-\left(\frac{b}{2}\right)^2\right] \tag{31b}$$

$$\tau_{xy} = -z(C_{16}w_{,xx}+2C_{16}\phi_{,x}) \tag{31c}$$

As shown, τ_{xz} satisfies the contour boundary condition at $z = \pm b/2$ [see eqn (11)]. However, since τ_{xy} is not a function of y, the contour boundary condition requires $\tau_{xy} = 0$. This yields again the twist-bending curvature relations of $\phi_{,x}/w_{,xx} = -C_{16}/2C_{66}$ and therefore supplies additional indication that eqn (28) represents the bending–torsion coupling mechanism in symmetric beams. In addition, the differential equilibrium equation [eqn (6)] yields

$$w_{,xxx} = -\frac{12F_z^t}{ab^3}\frac{C_{66}}{C_{11}C_{66}-C_{16}^2} \tag{32}$$

The natural boundary conditions at the beam tip [eqn (10)] show that $w_{,xx}(l) = 0$ there. Carrying out the longitudinal integrations of $w_{,xx}$, $w_{,x}$, w and ϕ for a clamped–free beam, yields a "strength of materials" type of solution for the resulting bending and twist:

$$w = \frac{2F_z^t}{ab^3}\frac{C_{66}}{C_{11}C_{66}-C_{16}^2}x^2(3l-x) \tag{33a}$$

$$\phi = -\frac{3F_z^t}{ab^3}\frac{C_{16}}{C_{11}C_{66}-C_{16}^2}x(2l-x) \tag{33b}$$

Using the nondimensional parameters $\tilde{x} = x/l$, $\tilde{y} = 2y/a$, $\tilde{z} = 2z/b$, $\tilde{a} = a/l$, $\tilde{b} = b/l$ and $\tilde{C}_{ij} = C_{ij}/C_{11}$, the warping in this case may be expressed as [see eqn (30)]

$$\frac{\Psi}{F_z/4aC_{55}} = \tilde{z}(3-\tilde{z}^2)+\frac{6\tilde{a}}{\tilde{b}^2}\frac{\tilde{C}_{16}\tilde{C}_{55}}{\tilde{C}_{66}-\tilde{C}_{16}^2}(\tilde{x}-1)\tilde{y}\tilde{z} \tag{34}$$

The above expression clearly demonstrates the three-dimensional nature of the warping. While the first term of eqn (34) represents the well-known "isotropic warping", the second term represents the twist–bending coupling and is therefore proportional to the bending curvature along the beam [see eqns (28) and (30)]. Figure 5 presents the warping distributions for the mid-span of a beam of rectangular cross-section due to a tip beamwise load. The warping distribution over the beam tip is identical to the "isotropic" distribution since no bending curvature–twist coupling takes place at that point. Figure 6 presents the warping for three values of $\tilde{x}$. As shown, in inboard cross-sections ($\tilde{x} < 1$), the second term in eqn (34) overshadows the first term (which is the only contributor when $\tilde{x} = 1$).

3.3.2. *A tip edgewise force* (F_y^t). In this case, an exact analytic solution may be derived by assuming $w = \phi = 0$, and warping of the following shape:

$$\Psi = -\frac{6F_y^t}{a^3bC_{66}}\left[\frac{y^3}{3}-\left(\frac{a}{2}\right)^2 y\right]+\alpha y^3+\beta(x-l)\left(y^2-\frac{a^2}{12}\right)+\gamma y \tag{35}$$

where

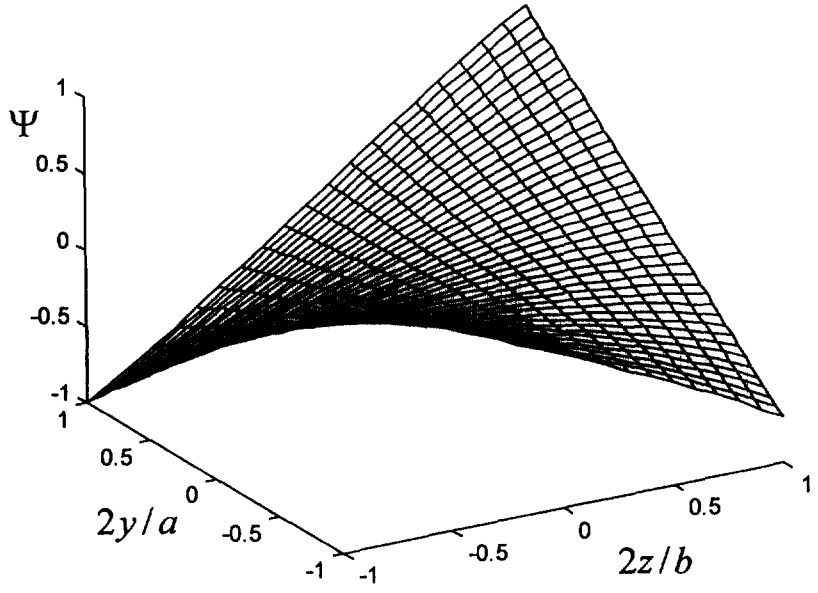

Fig. 5. The warping distribution over the mid-span cross-section due to a tip beamwise load. The solid cross-seection is a rectangular defined by the lines $y = \pm a/2$ and $z = \pm b/2$.

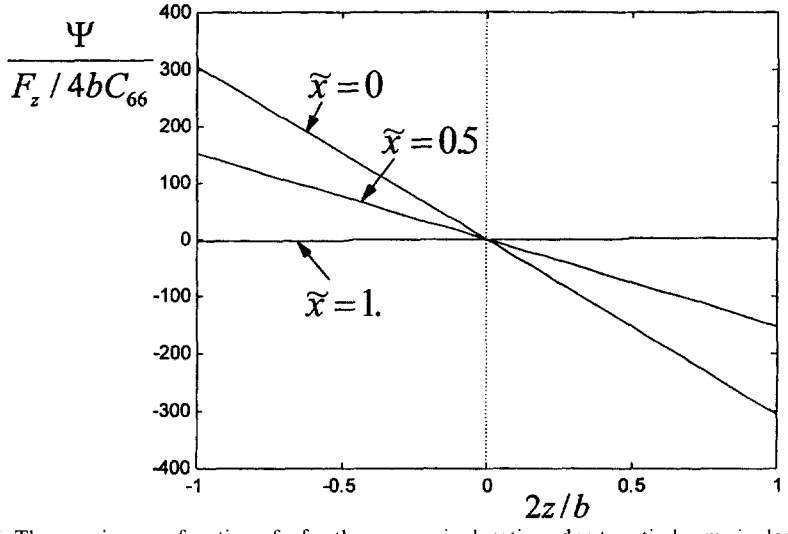

Fig. 6. The warping as a function of z for three spanwise locations due to a tip beamwise load. In this case, $2y/a = 1$, $a/l = 0.0667$ and $b/l = 0.0333$.

$$\alpha = -\frac{C_{16}}{3C_{66}}\beta \tag{36a}$$

$$\beta = \frac{C_{16}}{2C_{66}}\frac{v_{,xx}}{x-l} \tag{36b}$$

$$\gamma = \frac{C_{16}}{C_{66}}\left(\frac{a^2\beta}{12} - u_{,x}\right) \tag{36c}$$

It is also assumed (and will be proved to be correct later on) that $v_{,xx}$ is proportional to

$(x-l)$, and that $u_{,x}$ is a constant. Therefore α, β and γ are all constants. Accordingly, Ψ is a function of both x and y. Using eqns (1a–c) and (3) it is possible to show that

$$\sigma_{xx} = \frac{C_{11}C_{66}-C_{16}^2}{C_{66}}\left[u_{,x}-yv_{,xx}+\beta\left(y^2-\frac{a^2}{12}\right)\right]-\frac{6F_y^t C_{16}}{a^3 b C_{66}}\left[y^2-\left(\frac{a}{2}\right)^2\right] \tag{37a}$$

$$\tau_{xz} = 0 \tag{37b}$$

$$\tau_{xy} = -\frac{6F_y^t}{a^3 b}\left[y^2-\left(\frac{a}{2}\right)^2\right] \tag{37c}$$

Equations 37(b, c) show that the contour boundary condition [eqn (11)] is satisfied. Using these stresses, the differential equilibrium equation [eqn (6)] yields

$$v_{,xxx} = -\frac{12F_y^t}{a^3 b}\frac{C_{66}}{C_{11}C_{66}-C_{16}^2} \tag{38}$$

while the natural boundary conditions at the beam tip [eqn (10)] show that

$$u_{,x} = -\frac{F_y^t}{ab}\frac{C_{16}}{C_{11}C_{66}-C_{16}^2} \tag{39}$$

Proper integrations using the boundary conditions of eqn (9) yields

$$v = \frac{2F_y^t}{a^3 b}\frac{C_{66}}{C_{11}C_{66}-C_{16}^2}x^2(3l-x) \tag{40a}$$

$$u = -\frac{F_y^t}{ab}\frac{C_{16}}{C_{11}C_{66}-C_{16}^2}x \tag{40b}$$

Using the nondimensional values defined for eqn (34), the warping in this case may be expressed as

$$\frac{\Psi}{F_y/4bC_{66}} = \tilde{y}(3-\tilde{y}^2)+\frac{\tilde{C}_{16}^2}{\tilde{C}_{66}-\tilde{C}_{16}^2}\left[\tilde{C}_{16}\tilde{y}(\tilde{y}^2+1)+\tilde{C}_{66}\frac{2}{\tilde{a}}(1-\tilde{x})(3\tilde{y}^2-1)\right] \tag{41}$$

The second term of eqn (41) is the warping due to the composite induced couplings. Similar to the second term of eqn (34), the warping in this case is also a function of the longitudinal coordinate x. Figure 7 presents the warping distribution as a function of y over three spanwise locations. As shown, the parabolic behavior of the second term in eqn (41) dominates this distribution.

4. ANALYTIC SOLUTIONS FOR BEAMS OF THIN-WALLED CROSS-SECTIONS

The analytic solutions presented in this section are for two types of thin-walled rectangular cross-sections. In the first case, an antisymmetric cross-section is obtained by homogeneous cross-section (i.e. constant elastic moduli). In the second case, non-homogeneous cross-section is used to create a representative symmetric lamination mode.

4.1. *Antisymmetric thin-walled beam undergoing tip torsional moment and axial force*

The following modeling of antisymmetric thin-walled beam is based on a single cell cross-section of arbitrary geometry, constant wall thickness and constant elastic moduli. When such a beam is subjected to a tip torsional moment (M_x^t) and a tip axial force (P^t),

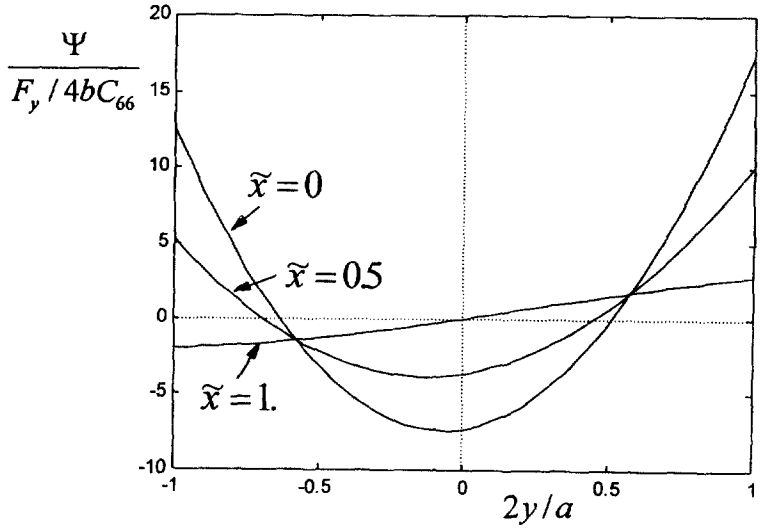

Fig. 7. The warping as a function of y for three spanwise locations due to a tip edgewise load ($a/l = 0.01$).

an exact analytic solution may be generated by assuming $v = w = 0$ and constant strains $\varepsilon_{\xi\xi}$ and $\gamma_{\xi\eta}$ over each cross-section and along the beam. Consequently, $\sigma_{\xi\xi}$ and $\tau_{\xi\eta}$ are also constants and Ψ is a function of s only. Then, eqn (7) shows that

$$P^{\mathrm{t}} = pt\sigma_{\xi\xi} \tag{42a}$$

$$M_x^{\mathrm{t}} = -2A_{\mathrm{m}}t\tau_{\xi\eta} \tag{42b}$$

where p is the cross-sectional circumference and A_{m} is the area enclosed by the median line. Since $\sigma_{\xi\xi}$ and $\tau_{\xi\eta}$ are constants, the differential equilibrium equation [eqn (8)] is satisfied. Substituting eqns (2a, b) and (4) in eqns (42a, b) yields two equations for the unknowns $u_{,x}$ and $\gamma_{\xi\eta}$. In this system, $\gamma_{\xi\eta}$ is replaced by $\phi_{,x}$ by integrating eqn (2b) under the condition $\oint \Psi_{,s}\,\mathrm{d}s = 0$, which yields $\gamma_{\xi\eta} = -2A\phi_{,x}/p$. Solving the above equations yields

$$\begin{pmatrix} u_{,x} \\ \phi_{,x} \end{pmatrix} = \frac{1}{C_{11}C_{66} - C_{16}^2} \begin{bmatrix} \dfrac{C_{66}}{pt} & \dfrac{C_{16}}{2A_{\mathrm{m}}t} \\ \dfrac{C_{16}}{2A_{\mathrm{m}}t} & \dfrac{C_{11}p}{4A_{\mathrm{m}}^2t} \end{bmatrix} \begin{pmatrix} P^{\mathrm{t}} \\ M^{\mathrm{t}} \end{pmatrix} \tag{43}$$

Having $u_{,x}$ and $\phi_{,x}$, the variation of Ψ as a function of s is obtained by integrating eqn (2b) (i.e. $\Psi_{,s} = -r\phi_{,x} - \gamma_{\xi\eta}$) under the condition $\oint \Psi\,\mathrm{d}s = 0$. Hence, the extension–twist coupling in thin-walled antisymmetric beams is represented by the off-diagonal terms in the matrix of eqn (43). As shown, $\phi_{,x} = (p/2A_{\mathrm{m}})(C_{16}/C_{66})u_{,x}$ in the case of a tip axial force, and $u_{,x} = (2A_{\mathrm{m}}/p)(C_{16}/C_{11})\phi_{,x}$ in the case of a tip torsional moment.

Similar to the case of solid cross-section, for a given set of elastic moduli, it is possible to define an "uncoupled case" where $C_{16} = 0$ and the values of C_{11} and C_{66} are kept unchanged [C_{55} is not relevant in this case—see eqn (4)]. Equation (43) shows that the uncoupled torsional rigidity is given in this case by $D = 4A_{\mathrm{m}}^2tC_{66}/p$. Consequently, it may be shown that the variation of $D/D_{(\theta=0)}$ coincides with the one shown in Fig. 4 for infinitely high values of a/b. Moreover, eqn (43) shows that the ratio of the effective (coupled) torsional rigidity, D_{e}, to the torsional rigidity in the uncoupled case, D, is given by

$$\frac{D_e}{D} = 1 - \frac{C_{16}^2}{C_{11}C_{66}} \tag{44}$$

It is interesting to note that eqn (44) is identical to eqn (29) for $r_z = 2$. Thus, it may be concluded that the loss of torsional rigidity of antisymmetric thin-walled cross-section is independent of the ratio a/b, and identical to the case of infinitely symmetric thin solid cross-section (plate).

It is also easy to show that the behavior of $u_{,x}$ as a function of P^t, C_{ij} and the material area, $A = pt$, is identical to the one presented by eqn (14a) for symmetric solid beam.

4.2. *Symmetric thin-walled beam undergoing tip axial force*

To form a simple thin-walled symmetric beam, a single-cell rectangular cross-section that consists of two horizontal walls at $z = \pm b/2$ and two vertical walls at $y = \pm a/2$ was used. The wall thickness, t, is constant. The upper half of this cross-section (i.e. the part for which $z > 0$) is assumed to be characterized by the elastic moduli (C_{11}, C_{66} and C_{16}, while the lower half (i.e. the part for which $z < 0$) is characterized by C_{11}, C_{66} and $-C_{16}$.

For vanishing values of C_{16}, it is clear that $v = w = \phi = \Psi = 0$ and $u_{,x} = P^t/2C_{11}(a+b)t$, where P^t is the tip axial force. When a nonzero value of C_{16} is considered, the "additional" strains $\Delta\varepsilon_{\xi\xi} = \Delta u_{,x}$ and $\Delta\gamma_{\xi\eta} = -\Psi_{,s}$ should appear in order to provide the same stress distribution (and therefore, both equilibrium equations and boundary conditions will be satisfied). To generate an exact closed-form analytic solution for this case, Ψ is assumed to be given by

$$\begin{aligned} \Psi(s) &= \alpha[s - \tfrac{1}{2}(a+b)] \quad \text{for} \quad 0 \leqslant s \leqslant (a+b) \\ &= \alpha[\tfrac{3}{2}(a+b) - s] \quad \text{for} \quad (a+b) \leqslant s \leqslant 2(a+b) \end{aligned} \tag{45}$$

where α is a constant to be determined and s is a circumferential coordinate along the wall that is directed counterclockwise and its origin is located at $y = a/2$, $z = 0$. The requirement for zero additional stresses yields [see eqn (4)]

$$\Delta\sigma_{\xi\xi} = C_{11}\,\Delta u_{,x} - C_{16}\alpha = 0 \tag{46a}$$

$$\Delta\tau_{\xi\eta} = C_{16}(u_{,x} + \Delta u_{,x}) - C_{66}\alpha = 0 \tag{46b}$$

It should be emphasized that since the signs of both the elastic modulus C_{16} and $\Psi_{,s}$ are identical to the sign of the z coordinate for each point over the cross-section, eqns (46a, b) hold for the entire beam. Solving eqns (46a, b) yields the values of $\Delta u_{,x}$ and α as

$$\Delta u_{,x} = \frac{C_{16}^2}{C_{11}C_{66} - C_{16}^2} u_{,x} \tag{47a}$$

$$\alpha = \frac{C_{11}C_{16}}{C_{11}C_{66} - C_{16}^2} u_{,x} \tag{47b}$$

Thus, similar to the case of a symmetric solid beam undergoing tip axial force, the coupling in the present case induces additional axial strain and a warping distribution. It is interesting to note that eqns (14a) and (47a) are in complete agreement, although they were derived for solid and thin-walled symmetric beams, respectively.

5. OVERVIEW ON THE ELASTIC COUPLING

General overview on the findings presented by the above solutions are summarized in this section. Reciprocity shows that the elastic couplings appear in pairs, and therefore their simultaneous examination may clarify the involved coupling mechanisms.

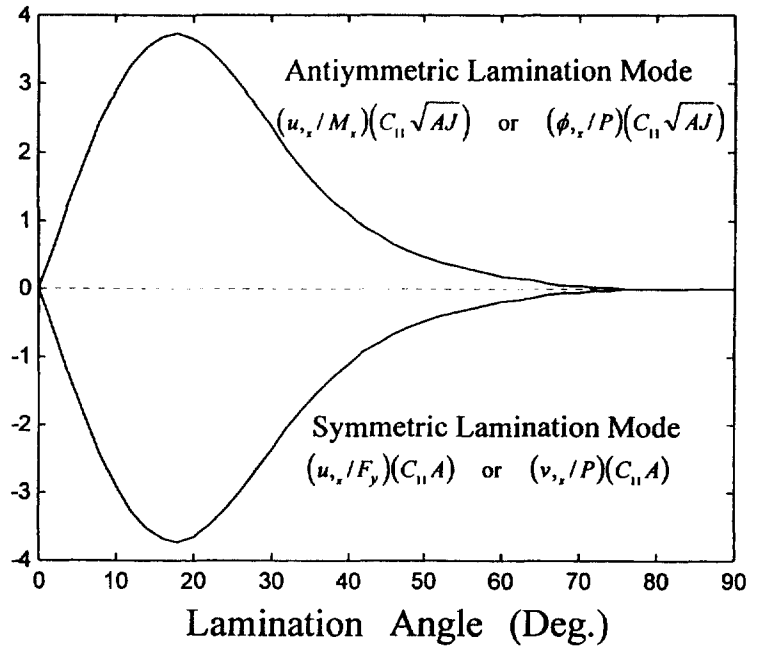

Fig. 8. The variation of the Extension-Twist coupling in antisymmetric beams and the Extension-Bending coupling in symmetric beams.

5.1. *Extension–bending coupling (symmetric beams)*

The extension–bending coupling presented in Section 3.1 for a beam of solid cross-section undergoing axial load may be expressed in terms of $(v_{,x}/P)(C_{11}A)$. As expected, this coupling magnitude is identical to the one obtained for edgewise force as presented in Section 3.3.2, namely $(u_{,x}/F_y)(C_{11}A)$. These quantities are presented in Fig. 8 as functions of the lamination angle for the material properties of Appendix A.

The solution presented above for the influence of a tip edgewise force, may be slightly generalized by replacing a^3b with $12I_{yy}$. Equations (38) and (39) show that the extension–bending coupling in this case may be written as

$$u_{,x} = \frac{I_{yy}}{A}\frac{C_{16}}{C_{66}}v_{,xxx} \tag{48}$$

which indicates that the axial extension is coupled with the edgewise bending curvature variation, and is also a function of the generalized geometric parameters I_{yy} and A. Figure 9 presents the variation of $(u_{,x}/v_{,xxx})(A/I_{yy})$ as a function of the lamination angle.

5.2. *Extension–twist coupling (antisymmetric beams)*

The solution presented by eqn (43) may be put in a more educating form. Recalling that in this case $J = 4A_m^2 t/p$ and $A = pt$, one may write

$$\begin{pmatrix} u_{,x} \\ \phi_{,x} \end{pmatrix} = \frac{1}{C_{11}C_{66} - C_{16}^2} \begin{bmatrix} \dfrac{C_{66}}{A} & \dfrac{C_{16}}{\sqrt{AJ}} \\ \dfrac{C_{16}}{\sqrt{AJ}} & \dfrac{C_{11}}{J} \end{bmatrix} \begin{pmatrix} P^t \\ M^t \end{pmatrix} \tag{49}$$

which clearly expose the quantities A, J and $\sqrt{AJ}$ that represent axial, torsional, and mixed axial-torsional stiffness as expected in this problem. Figure 8 presents the ratio $(u_{,x}/M_x)(C_{11}\sqrt{AJ})$ or $(\phi_{,x}/P)(C_{11}\sqrt{AJ})$ obtained in this case as a function of the lamination angle.

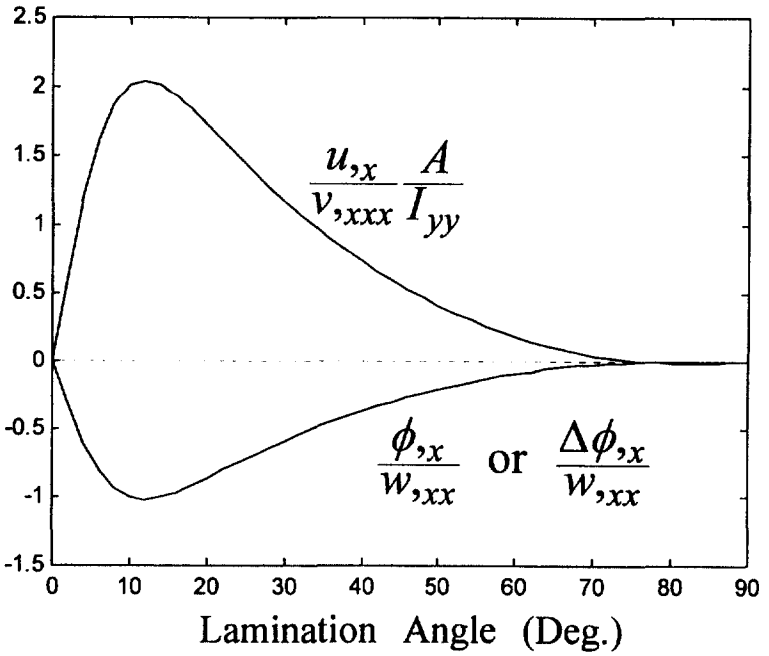

Fig. 9. The variation of the Bending-Twist coupling and the Extension-Bending coupling in symmetric beams.

5.3. *Bending–twist coupling (symmetric beams)*

The solution presented by eqns (20b, c) for the influence of a tip beamwise moment, $M_y^{\downarrow}$, shows that $\phi_{,x}/w_{,xx} = -C_{16}/2C_{66}$. Similarly, as indicated by eqn (28), this also turns to be the ratio between the additional twist and the beamwise curvature induced by the composite couplings in the case of a tip torsional moment. In addition, eqns (33a, b) show that the specific solution of a rectangular cross-section that undergoes a tip beamwise force generates the same ratio between the induced twist and the bending curvature. The above ratios are presented in Fig. 9 as functions of the lamination angle for the material properties of Appendix A.

It should be emphasized that the fact that ratio $-C_{16}/2C_{66}$ is not a function of the cross-sectional geometry is a consequence of the fact that the relevant solutions deal with homogeneous cross-sections. In a general multi-layered configuration, the above coupling magnitude are expected to be functions of geometrical properties as well.

6. CONCLUDING REMARKS

The present paper is focused on closed-form analytic solutions for composite beams. Numerous advantages are provided by these closed-form solutions. On top of their ability to provide a simple estimation of composite beam behavior due to various loads, they supply a clear physical explanation for the structural behavior and educating insight into the coupling mechanisms. They may also be used for identifying the critical parameters of various new configurations and subsequently, contribute to the efficiency of detailed analyses. Moreover, the warping distributions that are obtained by the present closed-form solutions may serve as the basic shape functions for detailed numerical schemes and thus, contribute to their adequacy.

REFERENCES

Ambartsumyan, S. A. (1964) Theory of anisotropic shells. NASA TTF-118.

Berdichevsky, E. A., Armanios, E. and Ashraf, B. (1992) Theory of anisotropic thin-walled closed-cross-section beams. *Composite Engineering* **2**(5-7), 411–432.

Bull, J. W. (ed.) (1995) *Numerical Analysis and Modelling of Composite Materials*, Chapter 1: Analysis of composite rotor blades. Chapman and Hall, London.
Chandrashekhara, K. and Bangera, K. M. (1992) Free vibration of composite beams using a refined shear flexible beam element. *Computers and Structures* **43**(4), 719–727.
Giavotto, V., Borri, M. and Mantegazza, P., Ghiringhelli, G., Carmaschi, V., Maffioli, G. C. and Mussi, F. (1983) Anisotropic beam theory and applications. *Computers and Structures* **16**, 402–413.
Kosmatka, J. B. and Friedmann, F. P. (1989) Vibration analysis of composite turbopropellers using a nonlinear beam-type finite element approach. *AIAA Journal* **27**(11).
Librescu, L. and Song, O. (1991) Behavior of thin-walled beams made of advanced composite materials and incorporating non-classical effects. *Applied Mechanics Review* **44**(11), Part 2.
Maiti, D. K. and Sinha, P. K. (1994) Bending and free vibration analysis of shear deformable laminated composite beams by finite element methods. *Journal of Composite Structures* **29**(1), 421–431.
Noor, A. K. and Burton, W. S. (1989) Assessment of shear deformation theories for multilayered composite plates. *Applied Mechanics Review* **42**(1).
Nosier, A. and Reddy, J. N. (1992) On vibration and buckling of symmetric laminated plates according to shear deformation theories. *Acta Mechanica* **94**, 123–169.
Ochoa, O. O. and Reddy, J. N. (1992) *Finite Element Analysis of Composite Laminates*. Kluwer Academic, Dordrecht.
Reddy, J. N. (1984) *Energy and Variational Methods in Applied Mechanics*. Wiley, New York.
Schmidt, R. and Librescu, L. (1994) Further results concerning the refined theory of anisotropic laminated composite plates. *Journal of Engineering Mathematics* 407–425.
Simon, L. (1981) A set of finite elements developed for the dynamic computation of composite helicopter blades. ONERA PT 1981–87.
Sokolnikoff, I. S. (1956) *Mathematical Theory of Elasticity*, 2nd edn. McGraw-Hill, New York.
Stemple, A. D. and Lee, S. W. (1989) A finite element modeling for composite beams undergoing large deflections with arbitrary cross sectional warping. *International Journal of Numerical Methods in Engineering* **28**(9), 2143–2163.
Tsai, S. W. and Hahn, H. T. (1980) *Introduction to Composite Materials*. Technomic, Westport, CT.
Yuan, K., Friedmann, P. P. and Venkatesan, C. (1994) Aeroelastic stability, response and loads of swept tip composite rotor blades in forward flight. *Proceedings of the 35th AIAA/ASME/ASCE/AHS/ASC Structures, Structural Dynamics and Materials Conference*, Hilton Head, SC.

APPENDIX A. MATERIAL PROPERTIES

The illustrative examples presented in this paper are based on typical transversely isotropic graphite/epoxy orthotropic laminae. As shown by Reddy (1984), the elastic properties may be expressed in terms of engineering constants, which in the present case are given by

$$E_{11} = 130 \times 10^9 \text{ N m}^{-2} \tag{A1a}$$

$$E_{22} = E_{33} = 12 \times 10^9 \text{ N m}^{-2} \tag{A1b}$$

$$G_{12} = G_{13} = 6 \times 10^9 \text{ N m}^{-2} \tag{A1c}$$

$$G_{23} = 4 \times 10^9 \text{ N m}^{-2} \tag{A1d}$$

$$\nu_{12} = \nu_{13} = 0.3 \tag{A1e}$$

$$\nu_{23} = 0.5 \tag{A1f}$$